Energetics of Electron-Transfer and Protonation Reactions of the Quinones in the Photosynthetic Reaction Center of *Rhodopseudomonas viridis*†

Björn Rabenstein, G. Matthias Ullmann, and Ernst-Walter Knapp*

Institut für Kristallographie, Fachbereich Chemie, Freie Universität Berlin, Takustrasse 6, D-14195 Berlin, Germany

Received August 4, 1997; Revised Manuscript Received December 9, 1997

ABSTRACT: The electron-transfer reactions involving the quinones in the bacterial photosynthetic reaction center (bRC) are coupled to a proton uptake by the bRC. In this study, we calculated the energies of the different states of the bRC occurring during these electron-transfer and protonation reactions by an electrostatic model. We considered the possibility that titratable groups of the bRC can change their protonation during these reactions. The protonation probabilities of titratable groups were obtained by a Monte Carlo calculation. In contrast to earlier studies by other groups, we used atomic partial charges derived from quantum-chemical calculations. Our calculated reaction energies are in agreement with experiments. We found that the proton uptake by the bRC is coupled more strongly to changes of the redox state of the quinones than to changes of their protonation state. Thus, the proton uptake by the bRC occurs predominantly before the protonation of Q_B. According to our computations, the reduction of $Q_B^{\bullet -}$ to the doubly negative state Q_B^{2-} is energetically even more unfavorable in the bRC than in solution. Therefore, we suggest that the second electron transfer from Q_A to Q_B occurs after Q_B has received its first proton. We found that the $Q_A^{\bullet -}Q_B^{\bullet -}$ state is more populated at pH 7.5 than the $Q_A^{\bullet -}Q_B^{\bullet}H$ state. The low population of the $Q_A^{\bullet -}Q_B^{\bullet}H$ state may be the reason why the singly protonated Q_B could not be detected spectroscopically. Our calculations imply that the first protonation of $Q_B^{\bullet -}$ is a prerequisite for the second electron transfer between Q_A and Q_B. Therefore, a pH dependence of the equilibrium between the states $Q_A^{\bullet -}Q_B^{\bullet -}$ and $Q_A^{\bullet -}Q_B^{\bullet}H$ can also explain the experimentally observed pH dependence of the rate for the second electron-transfer step. On the basis of our calculated reaction energies, we propose the following sequence for the electron-transfer and protonation reactions: (1) first electron transfer from Q_A to Q_B, (2) first protonation of Q_B (at the distal oxygen close to Ser L223), (3) second electron transfer from Q_A to Q_B, and (4) second protonation of Q_B (at the proximal oxygen close to His L190).

The bacterial photosynthetic reaction center (bRC)[1] is a pigment−protein complex in the membrane of purple bacteria. It converts light energy into electrochemical energy by coupling photoinduced electron transfer to proton uptake from cytoplasm. The crystal structure of the bRC from *Rhodopseudomonas (Rps.) viridis* (*1*−*3*) and from *Rhodobacter (Rb.) sphaeroides* (*4*, *5*) enabled a more detailed understanding of the various functional processes in the bRC. Four polypeptides form the bRC from *Rps. viridis*: the L, H, and M subunits and a tightly bound four-center *c*-type cytochrome. These polypeptides bind 14 cofactors: one carotenoid, four hemes, four bacteriochlorophylls, two bacteriopheophytins, one menaquinone (MQ), one ubiquinone (UQ), and one non-heme iron. Most of the cofactors arrange in two branches (A, B) related by a C_2 symmetry and extend from the special pair to the quinones. Only one branch (A) is electron-transfer active. Its cofactors are predominantly embedded in the L subunit. Electronic excitation of the special pair, a bacteriochlorophyll dimer, induces a multistep electron transfer from the special pair to Q_A, which is a MQ in the bRC from *Rps. viridis*. From there the electron moves to the Q_B, which is a UQ. After this initial reaction, a second electron transfer from Q_A to Q_B and two protonation reactions of Q_B follow, resulting in a dihydroquinone Q_BH_2. The dihydroquinone leaves its binding site and is replaced by an oxidized UQ from the quinone pool. The temporal order of these reactions is, however, not completely resolved (for a review see ref *6*). Recently, Graige *et al.* (*7*) proposed several models for the coupling of the protonation of Q_B to the electron transfer between Q_A and Q_B. On the basis of their kinetic data, they favored either a mechanism in which the second electron transfer to Q_B occurs in a concerted manner with the first protonation of Q_B or a mechanism in which the first protonation of Q_B precedes the second electron transfer. The dihydroquinone Q_BH_2 has two acidic protons, one at the quinone oxygen atom proximate to the non-heme iron (near His L190) and the other at the quinone oxygen atom distant from the non-heme iron (near Ser L223). Thus, there are two possibilities for the first protonation of Q_B.

In previous studies, we investigated several electron-transfer and binding reactions of photosynthetic proteins by

† This work was supported by the Deutsche Forschungsgemeinschaft SFB 312, Project D7. G.M.U. is supported by a Boehringer Ingelheim Fonds fellowship.

* Corresponding author: e-mail knapp@chemie.fu-berlin.de; fax +49-30-8383464.

[1] Abbreviations: bRC, bacterial (photosynthetic) reaction center; DMF, dimethylformamide; MC, Monte Carlo; MQ, menaquinone; UQ, ubiquinone.

S0006-2960(97)01921-1 CCC: $15.00
Published on Web 02/03/1998

various theoretical methods (*8*−*13*). In this work, we apply a continuum electrostatic method based on the Poisson−Boltzmann equation (*14*−*19*) to calculate the reaction energies of the electron-transfer and protonation reactions of the quinones in the bRC. Electrostatic calculations at the bRC were already done before (*20*−*22*). These studies focused on the titration behavior of the bRC before and after electron transfer from Q_A to Q_B. However, the energetics of the electron-transfer and protonation reactions of the quinones were not considered (*20*, *21*) or were only considered for the first electron transfer from Q_A to Q_B (*22*). Our goal in this work is to investigate the coupling between the protonation reactions and the electron-transfer reactions in the bRC. First, we determine the protonation patterns of the bRC when the quinones are in their various redox and protonation states. Subsequently, we compute the reaction energies of the electron-transfer and protonation reactions. In these calculations we consider all those protonation states that are energetically accessible. On the basis of our calculated reaction energies, we propose the energetically most favorable temporal order of the electron-transfer and protonation reactions. This is to our knowledge the first theoretical study in which the energetics not only of the first electron-transfer reaction between Q_A and Q_B but also of the second electron-transfer reaction between these quinones and of the two protonation reactions of Q_B are considered. Our results agree with experiments and can explain observed effects.

MATERIALS AND METHODS

Structure. In our calculations, we used the crystal structure of the bRC from *Rps. viridis* with a resolution of 2.3 Å (ref *2*; PDB entry 1prc). Since the cytochrome *c* subunit is more than 25 Å away from the quinone binding sites, we neglected this subunit in our calculations. All water molecules, sulfate ions, and detergent molecules were removed. The influence of water was considered exclusively by a higher dielectric constant in cavities and outside the protein. In some recent applications, selected water molecules were explicitly included in pK_a calculations (*20*, *23*, *24*). These calculations yielded results different from those obtained without explicit water molecules. Different selection schemes for the water molecules were applied. Only a few crystal water molecules, all crystal water molecules, or even additional solvent molecules were included. For hen egg lysozyme, the agreement between calculated and measured pK_a values was better without explicit water molecules (*24*). Calculations without explicit water may agree better with experiments because the orientation of water molecules is not known from X-ray crystallography but is needed for these calculations. Since the orientation of water molecules is uncertain, we decided to remove all water molecules. We used an extended atom representation for most nonpolar hydrogen atoms, except for the quinones, the chlorophylls, and the pheophytins, for which all hydrogens were treated explicitly. Coordinates of explicitly treated hydrogen atoms were generated with CHARMM (*25*). The positions of hydrogen atoms were energetically optimized, while the heavy atom positions were fixed.

In the crystal structure used, the Q_B binding pocket is occupied to only 30% (*2*). A structure with improved occupancy and resolution at the Q_B site has been solved but is not available yet (*3*, *26*). Therefore, we manipulated the bRC structure (PDB entry 1prc) at the Q_B site according to information from Lancaster *et al.* (*3*, *26*). We rotated Q_B around the axis through the methyl group at the quinone ring that is perpendicular to the ring plane, so that the methoxy group opposite to the methyl group shifted by 0.75 Å toward Ser L223. Furthermore, the carboxyl group of Glu L212 was rotated by 90° around the bond between C_γ and C_δ.

Atomic Partial Charges. Atomic partial charges of the amino acids, including the protonated and deprotonated state of titratable amino acids, were adopted from the CHARMM 21.3 parameter set. The acidic hydrogen atom of protonated glutamate and aspartate was not represented explicitly. Instead, appropriate charges at the two carboxyl oxygen atoms were assigned symmetrically. The atomic partial charges that are not included in the CHARMM 21.3 parameter set were calculated quantum-chemically with the program SPARTAN 4.0 (*27*). Using the CHELPG-like method (*28*) implemented in SPARTAN, we adjusted the atomic partial charges to represent the electrostatic potential calculated from the wave function faithfully. The atomic partial charges of chlorophylls and pheophytins were calculated semiempirically at the PM3 level; those of the quinones (in all possible redox and protonation states) and of the deprotonated cysteine were calculated by an ab initio method with a 6-31G** basis set. The atomic partial charges of high-spin non-heme iron (*29*) and its ligands were calculated by a density functional method (LSDA/VWN) implemented in SPARTAN using the DN** basis. The calculated partial charges of the iron center and the two quinones are listed in Tables S1−S3 (Supporting Information). The neurosporene and the isoprene tails of Q_A, chlorophylls, and pheophytins were not considered in the quantum chemical calculations. The atomic partial charges of these apolar groups were set to zero.

Calculation of Protonation Patterns. The protonation probability $\langle x_i \rangle$ of a titratable group i in a protein with n titratable groups is given by the thermodynamic average over all possible protonation states of this protein (*17*):

$$\langle x_i \rangle = \frac{\sum_{\vec{q}} x_i \exp\left[-\beta \sum_{\mu} \left(x_\mu \Delta G_{\mathrm{intr}/\mu} + \frac{1}{2} \sum_{\nu \neq \mu} q_\mu q_\nu W_{\mu\nu} \right) \right]}{\sum_{\vec{q}} \exp\left[-\beta \sum_{\mu} \left(x_\mu \Delta G_{\mathrm{intr}/\mu} + \frac{1}{2} \sum_{\nu \neq \mu} q_\mu q_\nu W_{\mu\nu} \right) \right]} \quad (1)$$

where $\beta = (k_B T)^{-1}$. The component q_i of the n -component protonation state vector $\vec{q}$ is the total charge of the titratable residue i, which can adopt the values −1 and 0 for acids or 0 and +1 for bases in their unprotonated and protonated states, respectively; x_i is unity if group i is protonated and zero if group i is unprotonated; $W_{\mu\nu}$ is the electrostatic interaction between the titratable groups μ and ν if both are charged. The outer sums run over all 2^n possible protonation state vectors $\vec{q}$, the sums in the exponential functions run over all titratable groups. The energy $\Delta G_{\mathrm{intr}/\mu}$ is the energy required to protonate group μ while all other titratable groups are in their uncharged protonation states. This energy $\Delta G_{\mathrm{intr}/\mu}$ is related to the so-called intrinsic pK_a value pK_{intr} of group μ as given in

Table 1: Total Protonation and Some Single-Site Protonations at pH 7.5[a]

state of quinones	histidine (tautomers)[b]				glutamate					total[c]		
	L211		M16									
	δ	ϵ	δ	ϵ	H45	H177	H234	L104	L212	this calculation	experimental values	other calculations
Q_BQ_B	0.47	0.53	0.25	0.73	0.05	0.03	0.27	1.00	0.99	0.00	0.00	0.00
$Q_A^{\bullet -}Q_B$	0.50	0.50	0.25	0.72	0.06	0.06	0.30	1.00	0.99	0.14	0.24[d]/0.34[e,f]	0.5[g,h]
$Q_AQ_B^{\bullet -}$	0.53	0.47	0.25	0.73	0.05	0.59	0.26	1.00	1.00	0.60	0.37[e]/0.90[f]	0.7[g]/0.5[h]
$Q_A^{\bullet -}Q_B^{\bullet -}$	0.53	0.47	0.25	0.73	0.06	0.80	0.27	1.00	1.00	0.88		
$Q_A^{\bullet -}Q_B^{\bullet}H_{dist}$	0.48	0.52	0.25	0.73	0.06	0.05	0.31	1.00	1.00	1.15		
$Q_A^{\bullet -}Q_B^{\bullet}H_{prox}$	0.48	0.52	0.25	0.73	0.06	0.07	0.30	1.00	0.98	1.14		
$Q_AQ_B^{2-}$	0.58	0.42	0.24	0.74	0.05	0.99	0.25	1.00	1.00	0.97		2.6[h]
$Q_AQ_BH_{dist}^{-}$	0.54	0.46	0.25	0.73	0.05	0.68	0.25	1.00	1.00	1.68	1.3[i]	
$Q_AQ_BH_{prox}^{-}$	0.52	0.48	0.24	0.74	0.05	0.65	0.25	1.00	1.00	1.65		
$Q_AQ_BH_2$	0.46	0.54	0.24	0.73	0.05	0.03	0.28	1.00	0.99	2.01	1.9[j]/2.1[i]	

[a] All residues within a distance of 25 Å from the quinones and with at least 0.05 proton deviation from standard protonation are shown, except N-termini of L and M chains, which are completely deprotonated in all states. Histidines protonated only at $N_{\epsilon 2}$ are considered to be in standard protonation and therefore are not included in the table. [b] Remaining part is protonated at $N_{\delta 1}$ and $N_{\epsilon 2}$. [c] Expressed as difference from the ground state. [d] *Rb. capsulatus* (*43*). [e] *Rb. sphaeroides (41*). [f] *Rb. sphaeroides* (*40*). [g] *Rb. sphaeroides* (*22*). [h] *Rps. viridis* (*21*). [i] *Rb. sphaeroides* Glu L212 → Gln mutant (*46*). [j] *Rb. sphaeroides* (*42*).

$$\Delta G_{intr} = \frac{-2.303\,(pK_{intr} - pH)}{\beta} \qquad (2)$$

The difference between the intrinsic pK_a values pK_{intr} and the pK_a values of model compounds in aqueous solution and also the interactions $W_{\mu\nu}$ between the groups μ and ν were calculated by a continuum electrostatic method using the program MEAD (*30*). This program solves the linearized Poisson−Boltzmann equation of a molecular system by a finite difference method (*31*). The model compounds of amino acids are the *N*-formyl *N*-methylamide derivatives of the respective amino acids in aqueous solution, whose pK_a values are known from experiments. The experimental pK_a values were taken from Bashford *et al.* (*32*). For cysteine, which is not present in the protein studied by Bashford *et al.* (*32*), we used a pK_a value of 8.5 for the model compound.

We performed focusing (*33*) in three steps. Initially, we used a 250 Å cube with a 2.5 Å lattice spacing centered at the protein, followed by a 60 Å cube with a 1.0 Å lattice spacing, and finally a 15 Å cube with 0.25 Å lattice spacing, both centered at the titratable group. We used an ionic strength of 100 mM, an ion exclusion layer of 2 Å, and a solvent probe radius of 1.4 Å. The dielectric constant in the protein was set to $\epsilon_p = 4$, and the dielectric constant of the solvent was set to $\epsilon_s = 80$. These parameter values are similar to those used by Bashford and Karplus (*30*) and also to those used in earlier calculations investigating the protonation of the bRC (*21*, *22*). We neglected the influence of the membrane, since calculations on the membrane protein bacteriorhodopsin with (*34*) and without (*23*) a membrane model yielded basically the same results.

The thermodynamic average in eq 1 cannot be calculated exactly since the number of possible protonation states of the bRC (2^n with $n \approx 200$) is far too large. Instead we used a Metropolis Monte Carlo (MC) method, implemented in the program MCTI (*19*). The statistical uncertainty of this method can be estimated by evaluating the protonation correlation function for each individual titratable group. To improve sampling efficiency, titratable groups coupled more strongly than 1.5 pK_a units changed their protonation state simultaneously in one MC move (*19*). Such simultaneous MC moves were done in addition to simple MC moves. In the unprotonated state of histidine two tautomers are possible. Both were considered in our calculations (*32*); hence we could calculate the fraction of ϵ and δ tautomers of histidines.

The protonation states of all titratable groups of the bRC were calculated separately for each of the 10 possible protonation and redox states of the quinone pair (column 1 of Table 1). Arginine, aspartate, cysteine, glutamate, histidine, lysine, tyrosine, and the C- and N-termini, if not formylated, were considered as titratable groups. The histidines coordinating the magnesium ions of the chlorophylls and also the glutamate and the histidines coordinating the non-heme iron were not considered as titratable groups. Explicit water molecules were not considered and hence were not included as titratable groups. Their pK_a values in aqueous solution, −1.7 and 15.7, are rather extreme. We do not expect that the protein is able to stabilize H_3O^+ or OH^- ions. Although ionized water molecules may participate as transient states in proton transfer, their presence in equilibrium states, which we investigate in this study, is unlikely. In total, 194 titratable groups were included in the calculations.

The MC sampling was done at pH 7.5 and 300 K. One MC scan comprises as many random individual protonation changes (MC moves) as there are titratable groups considered. We did at first 3000 MC scans. Then we fixed the protonation of all groups whose protonation probability differed from unity or zero by less than 10^{-6} in their respective protonation states and excluded these groups from further MC sampling. With this reduced set of titratable groups we performed another 7000 MC scans. This more efficient MC method is also implemented in the program MCTI. The sampling was sufficient to reach a standard deviation of less than 0.01 proton at each individual titratable group. In general, the standard deviation of a single group was much smaller than 0.01. The sum of the standard deviations of all protonation probabilities was for each state about 0.02 proton.

Redox Potentials and pK_a Values of the Quinones in Solution. The continuum electrostatic method is capable of yielding reliable values merely for differences of reaction energies in different electrostatic environments. For that reason, our calculation required pK_a values and redox potentials of MQ and UQ in aqueous solution as reference for computing the reaction energy of electron-transfer and

protonation reactions in the bRC. Both quinones, however, are not soluble in pure water. Swallow (*35*) and Morrison *et al.* (*36*) extrapolated the pK_a values of the quinones from pK_a values of water-soluble quinone derivatives taking into account the effect of different quinone ring substituents on the pK_a value. The resulting pK_a values are 4.9 for $UQ^{\bullet -}$/$UQ^{\bullet}H$ and 11.7 for UQH^-/UQH_2.

Redox potentials of quinones cannot be measured in a protic solvent, since a reduced quinone will inevitably take up a proton. Redox potentials in aprotic solvents, however, are known: $MQ/MQ^{\bullet -}$ in DMF (dimethylformamide), −709 mV; $UQ/UQ^{\bullet -}$ in DMF, −602 mV (*37*); and $UQ^{\bullet -}/UQ^{2-}$ in acetonitrile, −1450 mV (*36*).

We corrected the redox potentials of the quinones obtained in nonaqueous solutions to get redox potentials in aqueous solutions by accounting for the different solvation energies in the respective solvents. For that purpose, we calculated the energy for dissolving the quinones in their different redox states in water, acetonitrile, and DMF by the continuum electrostatic method (*38*). In the calculations, the following solvent parameters were used: The dielectric constants are $\epsilon = 80$ for water, $\epsilon = 38$ for acetonitrile, and $\epsilon = 37$ for DMF (*39*). The solvent radii are 1.4 Å for water, 2.0 Å for acetonitrile, and 2.8 Å for DMF. Finally, we obtained the following redox potentials of the quinones in aqueous solution: −699 mV for $MQ/MQ^{\bullet -}$, −592 mV for $UQ/UQ^{\bullet -}$, and −1420 mV for $UQ^{\bullet -}/UQ^{2-}$.

Energetics of Electron Transfer and Protonation. Titratable groups that have a protonation probability of less than 0.05 or more than 0.95 after MC titration in all considered bRC states are assumed to contribute to the thermodynamic average in eq 1 only in their totally deprotonated or protonated states, respectively. Therefore, we fixed those titratable groups in the totally deprotonated or protonated state and did not consider them as titratable groups in subsequent calculations. Only five titratable groups had variable protonations at pH 7.5 according to this criterion. These residues are aspartate M182 and the glutamates H45, H177, H234, and M76. To test whether fixing the protonation state of nearly completely protonated or unprotonated residues is justifiable, we repeated the calculation of protonation patterns state with this reduced set of unfixed titratable groups. The difference between the protonation probability in this calculation and the calculation with the full set of titratable groups was less than 0.05 for each of the five residues with variable protonations.

We calculated the energy of the protonation reactions of Q_B by the same continuum electrostatic method as before. Now, in addition to the five titratable groups with variable protonations, Q_B was also considered as a titratable group. Since the number of titratable group was small in this calculation, no MC sampling was necessary and the thermodynamic average (eq 1) could be calculated exactly. The exact evaluation of eq 1 prevents sampling problems, which may occur with MC sampling if the protonation energy of Q_B is too large. The protonation energy was obtained from the protonation probability $\langle x \rangle$ of Q_B by

$$\Delta G = -\frac{1}{\beta} \ln \frac{\langle x \rangle}{1 - \langle x \rangle} \qquad (3)$$

The reaction energy of electron transfer from Q_A to Q_B was obtained similarly to the calculation of the protonation probability. The two quinones were included in the calculation as a redox pair. Therefore, the pH-dependent protonation energy ΔG_{intr} defined in eq 2 was substituted by the pH-independent redox potential difference between the two quinones when all titratable groups with variable protonations are in their uncharged states. The redox potential difference between the two quinones in the protein is obtained by a continuum electrostatic method as a shift of the redox potential difference when the quinones are transferred from aqueous solution into the protein. The corresponding value $\langle x \rangle$ characterizes the equilibrium distribution of the states before and after electron transfer. The reaction energy of the electron transfer is obtained as before from $\langle x \rangle$ by eq 3.

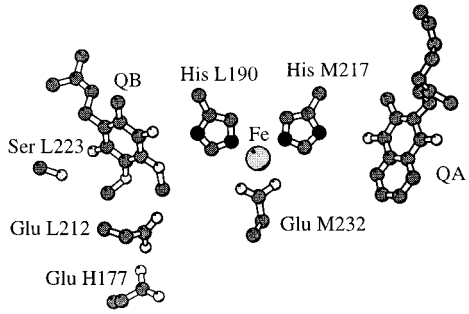

FIGURE 1: Structural arrangement of the quinone binding pockets. View of the two quinones, the non-heme iron with ligands (His L230 and His M264 are omitted for the sake of clarity), and nearby putatively functional residues. Glu L212 is almost completely protonated in all states at pH 7.5. At Glu H177 most of the total protonation changes are localized. Ser L223 is important for the first proton transfer. The oxygen atom of Q_B pointing toward and away from the non-heme iron are called proximal oxygen atom and distal oxygen atom, respectively. [Drawn with the Molscript program (*55*).]

RESULTS AND DISCUSSION

Total Protonation and Protonation Patterns. Proton uptake by wild-type and mutant bRCs during electron-transfer and protonation reactions of the quinones were studied experimentally by several research groups (*40*−*43*). However, these investigations were done at the bRC from *Rb. sphaeroides* (*40*−*42*) and from *Rb. capsulatus* (*43*) but not from *Rps. viridis*. Much effort was spent to assign changes in total protonation to specific residues. One of the titratable groups in proximity to Q_B is Glu L212 (closest atom pair distance 3 Å; Figure 1). Mutation studies indicate a pK_a value of Glu L212 of 9.0−9.5 (*44*, *45*) and imply no participation of Glu L212 in proton uptake at pH 7.5 and below (*46*, *47*). However, time-resolved IR measurements suggest a protonation of Glu L212 after formation of $Q_B^{\bullet -}$ (*48*). The latter observation is supported by electrostatic calculations at the bRC from *Rb. sphaeroides* (*22*) and from *Rps. viridis* (*21*). In both theoretical studies, it is proposed that the protonation of Glu L212 contributes to a significant part to the total proton uptake by the bRC associated with $Q_B^{\bullet -}$ formation.

Using a continuum electrostatic method, we calculated the protonation patterns and the total protonation of the bRC for all possible states of the quinones as shown in Figure 2. In contrast to previous theoretical studies by other groups (*21*, *22*), we considered not only those bRC states in which the quinones are in different redox states but also those bRC states in which Q_B is protonated. Table 1 shows the

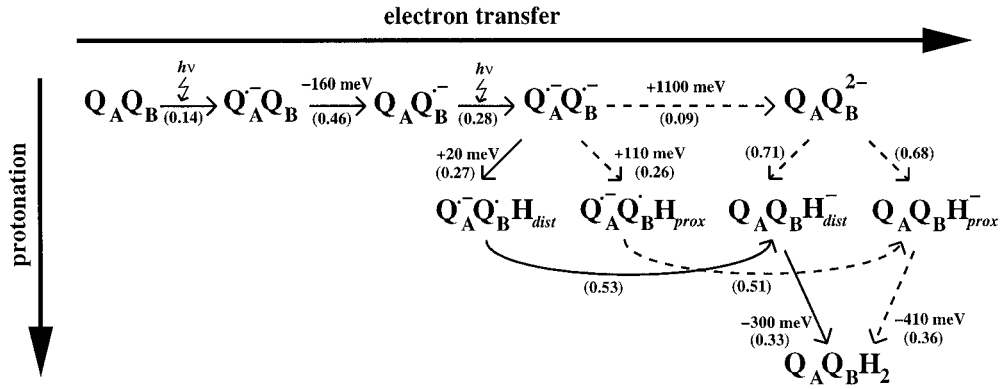

FIGURE 2: Scheme of the possible electron-transfer and protonation reactions involving the quinones of the bRC. Solid arrows are used for the energetically preferred reaction sequence. Calculated reaction energies are given near the respective arrows. Changes in total protonation during the reactions are given in parentheses.

protonation probability of nonstandard protonated residues that are less than 25 Å away from the quinones. Furthermore, the difference between the total protonation of the ground state Q_AQ_B of the bRC and the total protonation of the respective other states are listed in comparison to previous experimental and theoretical values. Our results imply that the proton uptake by the bRC occurs predominantly during the redox reactions of the quinones, whereas the proton uptake by the bRC coupled to the protonation of Q_B is smaller. The uptake of about 0.2 proton on average goes along with each of the two reductions of Q_A (Figure 2). With the exception of the electron transfer to the singly reduced, unprotonated Q_B, all electron transfers from Q_A to Q_B are coupled to an uptake of about 0.5 proton on average (Figure 2). The protonation of Q_B in the states $Q_A^{\bullet\,-}Q_B^{\bullet\,-}$, $Q_A^{\bullet\,-}Q_B^{\bullet}H_{dist}$, and $Q_A^{\bullet\,-}Q_B^{\bullet}H_{prox}$ induces an uptake of only about 0.3 proton on average (Figure 2). This means that an excess proton is already partially available in the protein matrix, before the protonation of Q_B actually occurs.

Our calculated changes of the total protonation are in reasonable agreement with the experimental results. However, the measured value of proton uptake depends sensitively on details of the experimental procedure, so that different groups got significantly different results (Table 1). Discrepancies between experiments and calculations may be explained by the following arguments: (i) Most experimental values are obtained from bRCs of purple bacteria other than *Rps. viridis*, which is explored in this study. (ii) Experimental values cannot easily be assigned to a specific bRC state, since often only the redox state and not the protonation state of the quinones is determined by experimental conditions. We assigned the experimental values of protonation changes to the states that are, according to our calculated energies (see below), occupied with the highest probability. In addition, experimental values from different groups vary. Some experiments indicate a coupling of the proton uptake by the protein matrix during the first electron transfer from Q_A to Q_B (*40*, *49*), while others do not (*41*). Our calculations suggest also a coupling of the first electron transfer between Q_A and Q_B to proton uptake by the protein matrix (Figure 2) and thus imply a pH dependence of this electron-transfer reaction.

Earlier electrostatic calculations by other groups tend to give higher values for total protonation differences with respect to the ground state Q_AQ_B than our calculations, especially for the state $Q_AQ_B^{2-}$. The differences between our results and those obtained by Beroza *et al.* (*22*) may be related to the different bRC considered in the calculations. Beroza *et al.* (*22*) used the bRC from *Rb. sphaeroides* while Lancaster *et al.* (*21*) and we used the bRC from *Rps. viridis*. The bRC structures used by Lancaster *et al.* and us are very similar, since we adjusted the structure of Deisenhofer *et al.* (*2*) according to the available information about the structure determined by Lancaster *et al.* (*3*, *26*). Thus, the most probable source for the discrepancies between their and our results are the different atomic partial charges. We used atomic partial charges derived from quantum-chemical calculations, for which the charge difference between the different protonation and redox states is distributed over all atoms of the respective quinone. Lancaster *et al.* (*21*) used atomic partial charges, for which the charge difference between different quinone redox states is exclusively localized at the carbonyl carbon and carbonyl oxygen atoms of the quinone ring. This more localized charge difference may explain the larger effects of the quinone redox states on the total protonation of the bRC.

Several titratable groups contribute to the proton uptake by the whole bRC, but most of them participate only with very small protonation changes. Besides the Q_B, the residue Glu H177 has the largest contribution to the proton uptake (Table 1). The distance of the carboxyl oxygen atom of this residue to the distal oxygen atom of Q_B is 8.0 Å (Figure 1). Glu H177 is possibly also involved in the proton-transfer pathway from the solvent to Q_B (*26*). According to our calculations, Glu L212 does not contribute significantly to the proton uptake at pH 7.5, since it is almost completely protonated for all redox and protonation states of Q_A and Q_B. This result is not in agreement with previous calculations (*21*, *22*), which suggest that Glu L212 is involved significantly in the proton uptake upon Q_B^- formation. However, the very small, but not vanishing, ionization probability of Glu L212 of 1−2% in the states in which Q_B is neutral shows that Glu L212 just starts to titrate at pH 7.5. The statistical uncertainty of the protonation probability of Glu L212 is less than 10^{-3} proton in our computation.

Our calculations support the above-mentioned experimental results (*44*−*47*) that Glu L212 is not ionized at pH < 7.5, but it is at least partially ionized and involved in proton uptake at pH > 7.5 (*46*, *47*). However, these results are obtained with the bRC from *Rb. sphaeroides* (*44*−*46*) and

from *Rb. capsulatus* (*47*) but not from *Rps. viridis*, which was used for the calculations. Our results cannot support the interpretation of the time-resolved IR measurements suggesting an involvement of Glu L212 in the proton uptake at pH 7.5 (*48*). Also, Hienerwadel *et al.* (*48*) discussed the uncertainty in assigning the observed spectroscopic effects to specific residues. According to our calculations, we would prefer an assignment to Glu H177. However, since Glu H177 and Glu L212 are strongly coupled (about 5 p*K* units), small changes in the protein environment may cause Glu L212 rather than Glu H177 to changes its protonation during Q_B reduction. Regardless of this uncertainty, a mutation of Glu L212 will influence the protonation behavior of Glu H177, since the carboxyl carbon atoms of the two residues are only 6.8 Å apart.

Energetics of Electron Transfer and Protonation. Using a continuum electrostatic model, we calculated equilibrium constants for selected electron-transfer and protonation reactions of the quinones. From these equilibrium constants we obtained the reaction energies. The calculated energy values are given in Figure 2 and will be discussed in the following sections.

(A) First Electron Transfer from Q_A to Q_B. Measured equilibrium constants for the first electron transfer from Q_A to Q_B in the bRC from *Rps. viridis* are 900 ± 50 at pH 6.0 and about 300 at pH 7.5 and 9.0 (*49*), which correspond to free energy changes of −175 and −150 meV, respectively. An earlier measurement gave an equilibrium constant of about 100 at pH 9.0 (*50*), which corresponds to a free energy change of −120 meV. Our continuum electrostatic calculations yielded an energy difference of −160 meV at pH 7.5. In the bRC from *Rb. sphaeroides* the measured reaction energy of the first electron transfer from Q_B to Q_B is about −70 meV (*51*, *52*). Recent continuum electrostatic calculations at the bRC from *Rb. sphaeroides* were not able to reproduce this value. The energy was obtained with the wrong sign and was 230 meV higher than the experimental value (*22*). This may be due to problems with the crystal structure of the bRC from *Rb. sphaeroides* or due to the atomic partial charges used, which were not obtained from quantum-chemical computations.

In a recent crystallographic study, conformational differences between the dark-state structure (Q_AQ_B) and the light-state structure ($Q_AQ_B^{\bullet -}$) of the bRC from *Rb. sphaeroides* were described (*53*). The Q_B environment of the light structure in this study is very similar to most other available structures of the bRC, which are believed to represent the dark state, *i.e.*, the Q_AQ_B state. However, one earlier bRC structure possesses a significantly different conformation at the Q_B binding site (*5*). Presumably, the Q_B in this structure is in the hydroquinone state (*3*). The putative hydroquinone-state structure (*5*) has very similar features at the Q_B site as the dark-state structure from Stowell *et al.* (*53*). In both structures, Q_B is rotated by about 180° and shifted by about 5 Å compared to the other bRC structures, which are supposed to be in the dark state. These similarities are surprising. Hence it seems not to be clear which conformational changes, if any, are important. In the present study, we did not consider conformational relaxation and fluctuation processes. In a more recent study, we used an iterative minimization scheme to calculate the redox potentials and the protonation energies for the various bRC states (manuscript in preparation). These minimizations, however, do not improve the present results.

(B) Second Electron Transfer from Q_A to Q_B and First Protonation of Q_B. Three different reactions may follow the first electron-transfer process: (i) the second electron transfer from Q_A to Q_B, (ii) the protonation at the proximal oxygen of Q_B, *i.e.*, the oxygen atom pointing toward the non-heme iron, or (iii) the protonation at the distal oxygen of Q_B, *i.e.*, the oxygen atom pointing away from the non-heme iron (Figure 2). Based on experimental results, different models were proposed. McPherson *et al.* (*46*) came to the conclusion that the first electron transfer is followed by the second electron transfer, whereupon the two protonations of Q_B occur. In contrast, the kinetic results of Graige *et al.* (*7*) fitted best to a model in which the first electron transfer is followed by the first protonation. Subsequently, the second electron transfer occurs as the rate-determining step. Another model, fitting the kinetic results of Graige *et al.* (*7*) almost as well, includes a concerted mechanism, in which the second electron and the first proton are transferred to Q_B simultaneously. The model derived from mutation studies of Paddock *et al.* (*54*) also supports a reaction sequence in which the first electron transfer from Q_A to Q_B is followed by the first protonation of Q_B, the second electron transfer from Q_A to Q_B, and finally by the second protonation of Q_B. In addition, the model of Paddock *et al.* (*54*) proposes that the first protonation occurs at the distal oxygen atom of Q_B and the second proton binds to the proximal oxygen atom.

We calculated the reaction energy for the second electron transfer from Q_A to Q_B and also for the first protonation of Q_B at the distal and at the proximal oxygen atom (Figure 2). The energy difference between the bRC states $Q_A^{\bullet -}Q_B^{\bullet -}$ and $Q_AQ_B^{2-}$ is +1100 meV. This energy difference is even higher than the energy difference between the respective quinone states in aqueous solution (720 meV). Thus, according to our calculations, a doubly reduced, unprotonated Q_B is unlikely to occur in the bRC. The protonation energy of Q_B in the bRC state $Q_A^{\bullet -}Q_B^{\bullet -}$ at pH 7.5 is also positive, but small (Figure 2). The protonation at the distal oxygen atom is energetically preferred by 90 meV. Therefore, we propose that after the first electron transfer from Q_A to Q_B, Q_B gets protonated at the distal oxygen atom. This is in agreement with the model of Paddock *et al.* (*54*). However, the difference between the protonation energies at the distal and proximal oxygen atom is small. If the protonation at the proximal oxygen is kinetically preferred, it may precede the protonation of the distal oxygen atom.

The energy of +20 meV for the first protonation of Q_B at the distal oxygen atom corresponds to a equilibrium partial protonation of about 30%. This fraction may be too small to detect the singly protonated Q_B spectroscopically. However, in the bRC from *Rb. sphaeroides*, the protonation of the singly reduced Q_B does not change (with a uncertainty of ±5%) in the pH range from 4 to 8 (footnote in ref *7*). One explanation for this behavior can be that the singly reduced Q_B is protonated less than 5% over this pH range. According to our calculations, the singly reduced Q_B has a protonation probability of about 30% at pH 7.5. This result does not contradict the experimental observation, if the protonation probability of the singly reduced Q_B remains constant at (30 ± 5)% over the pH range from 4 to 8. This may possibly be rationalized with a special titration behavior

of Q_B: Due to strong coupling of Q_B with titratable groups in the protein matrix, a nearly constant protonation probability of the singly reduced Q_B may be maintained over a wide pH range. The assumption of a nearly unprotonated singly reduced Q_B is not supported by our results. But it should be kept in mind that the experiments were done with the bRC from *Rb. sphaeroides*, while we used the structure of the bRC from *Rps. viridis* in our computation.

We found that the proton uptake by the bRC takes place before Q_B gets protonated. This may be one of the reasons for the experimental finding that the first protonation of Q_B is faster than the second electron transfer from Q_A to Q_B (*46*). Due to the fast protonation of Q_B, the system reaches the protonation equilibrium after the first electron-transfer process. The second electron is then transferred only if Q_B is protonated. If the protonation of Q_B depends on pH, this mechanism can explain the observed pH dependence of the second electron-transfer rate. This model is similar to the one derived from kinetic studies mentioned above (*7*).

(C) Second Protonation of Q_B. Measurements of the energies for the second protonation of Q_B at pH 9.0 and 9.5 gave $\geq (0 \pm 20)$ and $\geq (28 \pm 20)$ meV, respectively (*46*). Assuming a Henderson−Hasselbalch titration behavior, the protonation energy at pH 7.5 is −90 meV. This is in qualitative agreement with our calculated values of −300 and −410 meV (Figure 2). The discrepancy may be explained by the uncertainty of extrapolating the energy to lower pH values. Furthermore, the experiments were done at the bRC from *Rb. sphaeroides*, while we used the bRC from *Rps. viridis*. The results show that the state $Q_AQ_B\,H^-_{dist}$, in which Q_B is protonated at the distal quinone oxygen, is energetically more stable than the state $Q_AQ_BH^-_{prox}$. Hence, also in the doubly reduced state of Q_B, a protonated distal oxygen is preferred to a protonated proximal oxygen.

CONCLUSION

In this study, we investigated the coupling of the electron transfer between the quinones Q_A and Q_B in the bRC to the protonation of Q_B. We determined the protonation pattern and the total protonation of bRC states with the quinones in different redox and protonation states (Figure 2) by solving the Poisson−Boltzmann equation numerically. Furthermore, we calculated the reaction energies of the various electron-transfer and protonation processes. Unlike previous studies by other groups, we considered not only the electron-transfer reaction between the quinones, but also protonation reactions of the Q_B. Our results agree with models derived from experiments, which was not achieved in other theoretical approaches. Our success in reproducing experimental results is presumably mainly due to the use of atomic partial charges derived from quantum-chemical calculations. This was not done in previous calculations investigating the protonation of the bRC.

Our calculation of the total protonation of the various bRC states (Table 1) shows, that a large fraction of the proton uptake by the bRC is correlated to the electron-transfer processes between Q_A and Q_B. The actual protonation of Q_B goes along with a small increase of the total protonation of the bRC. This may explain why the protonations of Q_B are fast and hence are not rate-determining (*46*).

There is a controversy in the literature whether the residue Glu L212 close to Q_B (Figure 1) becomes protonated after electron transfer to Q_B or remains protonated during all reaction steps (*44*−*48*). According to our computations, Glu L212 is not directly involved in the proton uptake at pH ≤ 7.5. It may, however, be involved in the proton uptake at pH values higher than 7.5. This agrees with most experimental studies (*44*−*47*). The increase of the total protonation after electron transfer is mainly due to the protonation of Glu H177 (Table 1), which is also in proximity to Q_B (Figure 1).

The sequence of the electron-transfer and protonation reactions, *i.e.*, their temporal order, is not completely resolved experimentally. In particular, it is unclear if the first protonation of Q_B precedes the second electron transfer from Q_A to Q_B or not. Our calculated reaction energy for the reduction of the singly reduced Q_B to a doubly reduced Q_B is in the bRC is even higher than in aqueous solution. The reaction energy is larger than 1 eV. This energy is too large to make this state thermally accessible; thus the doubly reduced Q_B state does not occur in the bRC. Therefore, we conclude that the first protonation of Q_B precedes the second electron transfer between Q_A and Q_B. If the protonation of Q_B depends on pH, this mechanism can also explain the pH dependence of the second electron-transfer step (*7*), because the protonation of Q_B would be a prerequisite for the second electron-transfer step. According to our calculated reaction energies (Figure 2), we propose the following reaction sequence for the electron-transfer and protonation reactions of the quinones in the bRC: (1) first electron transfer from Q_A to Q_B, (2) first protonation of Q_B (at the distal oxygen close to Ser L223), (3) second electron transfer from Q_A to Q_B, and (4) second protonation of Q_B (at the proximal oxygen close to His L190). Whether the distal or the proximal quinone oxygen atom gets protonated first is, however, not certain, since the reaction energies do not differ much (Figure 2). Although the protonation of the distal oxygen atom is energetically favored, the protonation of the proximal oxygen atom can be faster if a proton is more easily available. However, experimental data also suggest that the protonation of the distal oxygen atom of Q_B precedes the protonation of the proximal oxygen atom (*54*). The energetically favored reaction sequence is shown with solid arrows in Figure 2. This reaction sequence is in agreement with several models derived from experiments (*7*, *54*). A mechanism in which the first protonation of Q_B and the second electron transfer occur simultaneously, *i.e.*, a concerted mechanism (*7*), would also agree with our calculations.

In future studies, mutant bRCs and bRCs from other purple bacteria, for which crystal structures with sufficient quality are available, will be investigated. For further improvement of the results, we plan to include conformational flexibility in our model.

ACKNOWLEDGMENT

We thank Dr. Donald Bashford, Dr. Paul Beroza, and Dr. Martin Karplus for providing the programs MEAD, MCTI, and CHARMM, respectively. We are grateful to Dr. Ingo Muegge and Dr. Werner Mäntele for useful discussions and to Dr. Liang Lou, who did calculations of atomic partial charges with different parameters (see Supporting Information).

SUPPORTING INFORMATION AVAILABLE

Figure S1 and Tables S1−S3, showing the calculated atomic partial charges of the iron center and of the two quinones in all occurring redox and protonation states (4 pages). Ordering information is given on any current masthead page.

REFERENCES

1. Deisenhofer, J., Epp, O., Miki, K., Huber, R., and Michel, H. (1985) *Nature 318*, 618−624.
2. Deisenhofer, J., Epp, O., Sinning, I., and Michel, H. (1995) *J. Mol. Biol. 246*, 429−457.
3. Lancaster, C. R. D., and Michel, H. (1996) in *The Reaction Center of Photosynthetic Bacteria* (Michel-Beyerle, M.-E., Ed.) pp 23−35, Springer, Berlin.
4. Allen, J. P., Feher, G., Yeates, T. O., Komiya, H., and Rees, D. C. (1987) *Proc. Natl. Acad. Sci. U.S.A. 84*, 6162−6166.
5. Ermler, U., Fritzsch, G., Buchanan, S. K., and Michel, H. (1994) *Structure 2*, 925−936.
6. Okamura, M. Y., and Feher, G. (1992) *Annu. Rev. Biochem. 61*, 861−896.
7. Graige, M. S., Paddock, M. L., Bruce, J. M., Feher, G., and Okamura, M. Y. (1996) *J. Am. Chem. Soc. 118*, 9005−9016.
8. Muegge, I., Ermler, U., Fritsch, G., and Knapp, E. W. (1995) *J. Phys. Chem. 99*, 89−100.
9. Ullmann, G. M., and Kostić, N. M. (1995) *J. Am. Chem. Soc. 117*, 4766−4774.
10. Muegge, I., Apostolakis, J., Ermler, U., Fritzsch, G., Lubitz, W., and Knapp, E. W. (1996) *Biochemistry 35*, 8359−8370.
11. Apostolakis, J., Muegge, I., Ermler, U., Fritzsch, G., and Knapp, E. W. (1996) *J. Am. Chem. Soc. 118*, 3743−3752.
12. Ullmann, G. M., Hauswald, M., Jensen, A., Kostić, N. M., and Knapp, E. W. (1997) *Biochemistry 36*, 16187−16196.
13. Ullmann, G. M., Knapp, E. W., and Kostić, N. M. (1997) *J. Am. Chem. Soc. 119*, 42−52.
14. Gilson, M. K., and Honig, B. H. (1986) *Biopolymers 25*, 2097−2119.
15. Nicholls, A., and Honig, B. (1991) *J. Comput. Chem. 12*, 435−445.
16. Davis, M. E., and McCammon, J. A. (1991) *J. Comput. Chem. 12*, 909−912.
17. Bashford, D., and Karplus, M. (1991) *J. Phys. Chem. 95*, 9557−9561.
18. Honig, B., and Nicholls, A. (1995) *Science 268*, 1144−1149.
19. Beroza, P., Fredkin, D. R., Okamura, M. Y., and Feher, G. (1991) *Proc. Natl. Acad. Sci. U.S.A. 88*, 5804−5808.
20. Cometta-Morini, C., Scharnagl, C., and Fischer, S. F. (1993) *Int. J. Quantum Chem., Quantum Biol. Symp. 20*, 89−106.
21. Lancaster, C. R. D., Michel, H., Honig, B., and Gunner, M. R. (1996) *Biophys. J. 70*, 2469−2492.
22. Beroza, P., Fredkin, D. R., Okamura, M. Y., and Feher, G. (1995) *Biophys. J. 68*, 2233−2250.
23. Sampogna, R. V., and Honig, B. (1994) *Biophys. J. 66*, 1341−1352.
24. Gibas, C. J., and Subramaniam, S. (1996) *Biophys. J. 71*, 138−147.
25. Brooks, B. R., Bruccoleri, R. E., Olafson, B. D., States, D. J., Swaminathan, S., and Karplus, M. (1983) *J. Comput. Chem. 4*, 187−217.
26. Lancaster, C. R. D., Ermler, U., and Michel, H. (1995) in *Anoxygenic Photosynthetic Bacteria* (Blankenship, R. E., Madigan, M. T., and Bauer, C. E., Eds.) pp 503−526, Kluwer Academic Publishers, Dordrecht, The Netherlands.
27. SPARTAN version 4.0. (1995) Wavefunction, Inc., Irvine, CA.
28. Breneman, C. N., and Wiberg, K. B. (1990) *J. Comput. Chem. 11*, 361−373.
29. Kartha, S., Das, R., and Norris, J. R. (1991) in *Metal Ions in Biological Systems* (Sigel, H., Ed.) Vol. 27, pp 323−359, Dekker, New York.
30. Bashford, D., and Karplus, M. (1990) *Biochemistry 29*, 10219−10225.
31. Warwicker, J., and Watson, H. C. (1982) *J. Mol. Biol. 157*, 671−679.
32. Bashford, D., Case, D. A., Dalvit, C., Tennant, L., and Wright, P. E. (1993) *Biochemistry 32*, 8045−8056.
33. Klapper, I., Fine, R., Sharp, K. A., and Honig, B. H. (1986) *Proteins*: *Struct., Funct., Genet. 1*, 47−59.
34. Bashford, D., and Gerwert, K. (1992) *J. Mol. Biol. 224*, 473−486.
35. Swallow, A. J. (1982) in *Function of Quinones in Energy Conserving Systems* (Trumpower, B. L., Ed.) pp 59−72, Academic Press, New York.
36. Morrison, L. E., Schelhorn, J. E., Cotton, T. M., Bering, C. L., and Loach, P. A. (1982) in *Function of Quinones in Energy Conserving Systems* (Trumpower, B. L., Ed.) pp 35−58, Academic Press, New York.
37. Prince, R. C., Dutton, P. L., and Bruce, J. M. (1983) *FEBS Lett. 160*, 273−276.
38. Sitkoff, D., Sharp, K. A., and Honig, B. (1994) *J. Phys. Chem. 98*, 1978−1988.
39. Lide, D. R. (1992) *CRC Handbook of Chemistry and Physics*, 73rd ed., CRC Press, Boca Raton, FL.
40. Maróti, P., and Wraight, C. A. (1988) *Biochim. Biophys. Acta 934*, 329−347.
41. McPherson, P. H., Okamura, M. Y., and Feher, G. (1988) *Biochim. Biophys. Acta 934*, 348−368.
42. McPherson, P. H., Okamura, M. Y., and Feher, G. (1993) *Biochim. Biophys. Acta 1144*, 309−324.
43. Sebban, P., Maróti, P., and Hanson, D. K. (1995) *Biochimie 77*, 677−694.
44. Paddock, M. L., Rongey, S. H., Feher, G., and Okamura, M. Y. (1989) *Proc. Natl. Acad. Sci. U.S.A. 86*, 6602−6606.
45. Takahashi, E., and Wraight, C. A. (1992) *Biochemistry 31*, 855−866.
46. McPherson, P. H., Schönfeld, M., Paddock, M. L., Okamura, M. Y., and Feher, G. (1994) *Biochemistry 33*, 1181−1193.
47. Miksovska, J., Maróti, P., Tandori, J., Schiffer, M., Hanson, D. K., and Sebban, P. (1996) *Biochemistry 35*, 15411−15417.
48. Hienerwadel, R., Grzybek, S., Fogel, C., Kreutz, W., Okamura, M. Y., Paddock, M. L., Breton, J., Nabedryk, E., and Mäntele, W. (1995) *Biochemistry 34*, 2832−2843.
49. Baciou, L., Sinning, I., and Sebban, P. (1991) *Biochemistry 30*, 9110−9116.
50. Shopes, R. J., and Wraight, C. A. (1985) *Biochim. Biophys. Acta 806*, 348−356.
51. Kleinfeld, D., Okamura, M. Y., and Feher, G. (1984) *Biochim. Biophys. Acta 766*, 126−140.
52. Mancino, L. J., Dean, D. P., and Blankenship, R. E. (1984) *Biochim. Biophys. Acta 764*, 46−54.
53. Stowell, M. H. B., McPhillips, T. M., Rees, D. C., Soltis, S. M., Abresch, E., and Feher, E. (1997) *Science 276*, 812−816.
54. Paddock, M. L., McPherson, P. H., Feher, G., and Okamura, M. Y. (1990) *Proc. Natl. Acad. Sci. U.S.A. 87*, 6803−6807.
55. Kraulis, P. J. (1991) *J. Appl. Crystallogr. 24*, 946−950.

BI971921Y